International Journal of Coal Geology 103 (2012) 51–59

Contents lists available at SciVerse ScienceDirect

International Journal of Coal Geology

journal homepage: www.elsevier.com/locate/ijcoalgeo

Correction to Klinkenberg slip theory for gas flow in nano-capillaries

Ebrahim Fathi [1], Ali Tinni, I. Yucel Akkutlu *

University of Oklahoma, United States

ARTICLE INFO

Article history:
Received 15 February 2012
Received in revised form 22 June 2012
Accepted 23 June 2012
Available online 20 July 2012

Keywords:
Klinkenberg
Lattice Boltzmann
Permeability
Shale
Nano-tube
Double-slip

ABSTRACT

Using a lattice Boltzmann (coarse grain) simulation of gas dynamics we show that the apparent permeability values of nano-scale capillaries could be significantly higher than those predicted by the Klinkenberg slip theory. The difference is due to kinetic effects of gas molecules that have gone through inelastic collisions with the capillary walls on those molecules that make up the bulk fluid in the capillary. The kinetic energy that the bouncing-back molecules have and the associated momentum carried to the bulk fluid is not a trivial matter in capillaries with diameter, h, less than 100 nm. Momentum carried by bouncing-back molecules amplifies the velocity profile developing across the diameter of the capillary. In a sense, it is not only the molecules interacting with the capillary wall that slip but also those interacting with the bulk fluid, i.e., double-slip. The double-slip effect is shown using measured permeability data of two crushed nano-porous samples, Pyrophyllite, and three different shale samples at varying pore pressures. Using the simulation results, we propose a modification to the Klinkenberg equation. Our new double-slip Klinkenberg equation includes a characteristic length scale (L_{Ke}) that is proportional to the kinetic energy per capillary cross-sectional area of the bouncing-back molecules by the capillary walls. The new length scale of the molecular kinetic effects in nano-capillaries is larger than the mean free path of the molecules. The double-slip Klinkenberg equation reduces to the classical equation for slip flow in large capillaries, i.e., $h/L_{Ke} >> 1$, and converges to the absolute permeability value at high pressure.

1. Introduction

Laboratory procedures for isothermal gas permeation lead to higher apparent permeability for porous samples. Explanation for this behavior was given by Klinkenberg in the 1940s in his seminal work that takes into account the phenomena of gas slippage (Klinkenberg, 1941). Accordingly, the steady-state flow rate through small capillaries is higher due to slippage of gas molecules by the capillary walls. In addition to the capillary size the slip is dependent on the type of permeating gas and the pore pressure; consequently, the measured permeability values for the sample could vary significantly. The Klinkenberg slip theory also yields a widely-known graphical technique that displays the measured permeability variations with respect to the reciprocal of the average pore pressure as a straight-line with an intercept equal to the absolute permeability of the sample and a slope related to mean free path of the gas molecules, Eq. (1) (Klinkenberg, 1941).

$$K_a = K\left(1 + \frac{b}{p}\right) \tag{1}$$

where K_a is the apparent permeability, K is the liquid permeability, b the slope of Klinkenberg straight line and p the pore pressure. Fig. 1 describes the molecular interactions between the gas and capillary wall molecules according to the Klinkenberg slip theory. While gas is flowing near the wall, consider that N number of molecules exist in the vicinity of the capillary wall. At any given time, N should be large enough such that, following their final collisions within the bulk fluid, N/2 molecules move towards the capillary wall while the other half moves away from the capillary wall due to their collisions with the wall molecules. According to the theory, the incoming molecules carry a non-zero velocity component parallel to the direction of bulk fluid flow. It is the macroscopic average of this velocity that is referred to as the slip velocity, i.e., $V_{slip} = (Vy_1 + Vy_2 + Vy_3 + \ldots + Vy_{,N/2})/(N/2)$. On the other hand, the other half of the molecules, the ones which have undergone inelastic collisions with the wall, are considered to move away from the wall with a zero velocity component parallel to the direction of the bulk fluid flow. Thus, according to the Klinkenberg's slip theory, only the incoming molecules from the bulk fluid can contribute to the total mass flux due to their slippage; the outgoing molecules, however, cannot influence the bulk fluid transport. In this article, we show that this assumption is reasonable when the capillaries are large enough for the formation of a bulk fluid, with infinite number of molecules, but it eliminates a possible kinetic role the bouncing-back molecules could play on the fluid flow in smaller capillaries.

In the following pages, we investigate the flow of gas through a model capillary using a numerical approach based on the lattice

* Corresponding author at: 100 East Boyd, Sarkeys Energy Center, Room 1210, Norman, OK 73019-1003, United States. Tel.: +1 405 325 8141; fax: +1 405 325 7477.
E-mail address: akkutlu@ou.edu (I.Y. Akkutlu).
[1] Now with the University of West Virginia.

0166-5162/$ – see front matter © 2012 Elsevier B.V. All rights reserved.
doi:10.1016/j.coal.2012.06.008

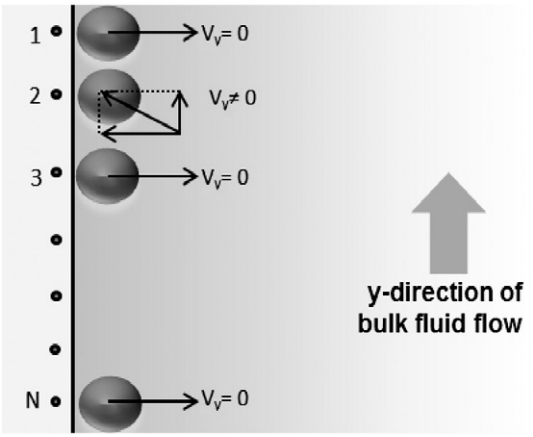

Fig. 1. Collisions of gas molecules with the capillary wall according to the Klinkenberg slip theory.

Boltzmann method (LBM). The method is described in detail in the Appendix A for the numerically-inclined reader. Briefly, we describe the capillary as a lattice (see Fig. 2) and allow the fluid particles (or coarse grains, which are fictitious meso-scale aggregates of the fluid molecules) to evolve on the lattice, traveling from node to node and interacting with each other and with the capillary wall as dictated by the Boltzmann's equation. Numerically, this is done by allowing the fluid particles to collide and stream locally in a repetitive manner, hence, transporting them from one end of the capillary to the other. This numerical process captures the gas dynamics well and, therefore, the approach has found many applications in various areas in physical sciences and engineering, in particular micro-fluidics (Succi, 2001; Sukop and Thorne, 2006). In our model, in addition to the Boltzmann forces dictating the manner the particles interact, cohesive forces are introduced between the neighboring particles. These additional forces enable us to capture the non-ideal behavior of the gas. Their influence is negligible at low pressures, however.

In the main body of this article, only the simulation results relevant to the steady-state gas flow in straight capillaries and to the slip theory will be discussed. The capillary size will be systematically reduced during the analysis. Unfortunately, this reduction in capillary size has computational limitations, since the accuracy of LBM decreases with the shrinking capillary, due to not having a statistically sufficient number of fluid particles at the lattice nodes at any time. This is the case for capillaries with diameter below 5 nano-meters (nm). We believe that non-equilibrium molecular simulation methods should be used at that scale. We leave such an investigation for a future study, and instead focus on capillaries with diameters between 5 and 100 nm. Within this diameter range, the kinetic effects of the molecules interacting with the capillary walls will be shown on fluid particle velocity profiles and kinetic energy plots as the evidence of deviations from the classical slip theory of Klinkenberg. We create Klinkenberg's permeability–pressure chart using our numerical data showing not only the flow regime where the classical Klinkenberg slip theory is valid, i.e. the straight line relationship prevails, but also a significant nonlinear deviation, which appears to be quadratic in average pressure of the capillary. These observations will be further supported experimentally by unsteady-state permeability measurements using crushed nano-porous samples: Pyrophyllite and three different organic-rich shale samples. Finally, based on the observations, we propose a modification to the Klinkenberg's equation, the so-called double-slip Klinkenberg equation, and discuss the common and new features of this equation.

2. Kinetic effect of gas–wall interactions on gas dynamics in a nano-capillary

At low Reynolds number values (in our case $N_{RE} \ll 1$), the flow of fluids in a capillary is described as laminar. For the laminar flow regime, the viscous coupling characteristically leads to a parabolic velocity profile across the capillary such that the value of velocity is the highest at the center and goes to zero (no-slip) by the walls. Fig. 3 showing this classical picture is also relevant for steady-state flow of super-critical methane in a 100 nm capillary at 2500 psi and 77 °F. The same velocity profile is predicted using both Poiseuille's law (analytical solution) and the LBM simulation indicating that the latter is accurately capturing the gas dynamics in the capillary.

However, the nature of gas flow changes when the average pressure inside the capillary is reduced. Fig. 4 clearly shows that the fluid velocity in nano-capillaries less than 50 nm is one to two orders of magnitude larger than that predicted using the classical theory when the average pressure is reduced to roughly below 500 psi. Also, smaller capillaries results in much higher fluid flow velocities than predicted by the Klinkenberg slippage theory. These observations are quite remarkable, raising serious concern in regards to the nature of dominant mechanism(s). Indeed, one would suspect that the accelerated flow is due to the gas slippage, but particularly in the case of capillaries under 50 nm one needs to be more careful because the variations in average velocity are significantly higher than what analytical methods and Klinkenberg's slip theory predicts (Klinkenberg, 1941). This can be clearly seen where the dimensionless permeability values obtained using crushed samples show much higher values than predicted using the Klinkenberg's slip theory. This indicates much higher gas

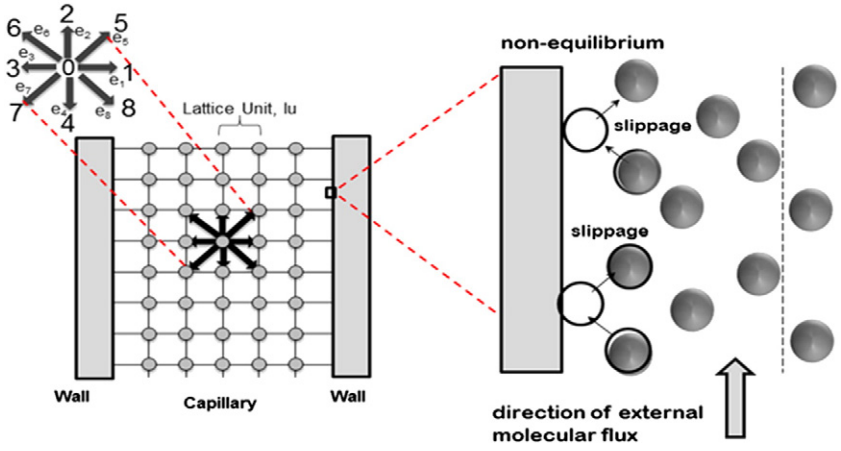

Fig. 2. Model nano-capillary represented as a D2Q9 lattice pattern (left) and with walls (right) that allow gas slippage.

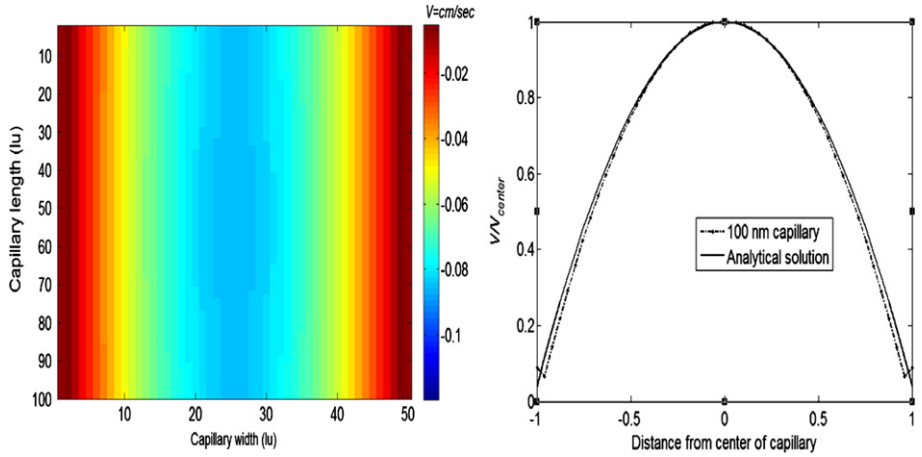

Fig. 3. left: Steady-state flow velocity distribution in 100 nm capillary at 2500 psi average pressure. Right: The normalized velocity profile across the capillary tube to the velocity at the center of the capillary, V/V_{center}.

flow velocities. Such higher gas velocities have been previously observed by King (2007), during gas flow in circular nanotubes.

A closer look into steady-state gas flow in nano-capillaries is possible by analyzing the numerical velocity profiles across each capillary. For this purpose, the data corresponding to 100 psi average pressure is chosen arbitrarily. Fig. 5 shows these velocity profiles. The figure also includes the analytical solution corresponding to flow in a 100 nm capillary, as the solid line, for comparison. Clearly, with the decreasing capillary size, the parabolic velocity profile is transformed into a uniform plug-like velocity profile at the central portion of the capillary. Furthermore, the estimated velocities by the wall are non-zero, suggesting that the flow experiences gas slippage. Interestingly, the estimated velocities near the wall are significantly higher than that at the center of the 20 nm capillary and the higher velocity values can be observed not only by the wall, but also deep into the capillary. Hence, the fluid flow behavior in a 20 nm capillary is fundamentally different than that in a 100 nm (or larger) capillary. The fundamental difference can be clearly observed in Fig. 6, where the kinetic energies associated with the bulk fluid particles are given for the same capillary sizes. Indeed, the kinetic energy associated with a bouncing-back molecule is dramatically higher in smaller capillaries.

The increased kinetic energy near the walls of smaller capillaries indicates that the dynamics of flow has changed. After their inelastic collisions with the wall, the bouncing-back molecules carry their corresponding momenta to the bulk fluid located at the central portion of the capillary and, hence, they create a molecular streaming effect on the bulk fluid flow. Thus, it is not only the gas molecules by the wall that slips, but also the bulk fluid 'wall', i.e., double-slip. The phenomenon of double-slip is new and certainly not part of the Klinkenberg's slip theory. As Fig. 7 shows, the double-slip effect leads to nonlinear deviation from the Klinkenberg slip theory (represented by the straight line) and is part of the measured apparent permeability for that capillary. These preliminary numerical results indicate that the kinetic effects of gas molecules interacting with the wall should be considered during the permeability measurement of nano-porous materials in the laboratory. In Fig. 7, we also include experimental data that belongs to Pyrophyllite, a naturally-occurring nano-porous material with isotropic mechanical properties. The experimental data also shows the existence of nonlinearity. The data is collected performing routine gas uptake measurements at various pressures once the sample is crushed into 5.68 mm size fragments. In the figure the experimental data is shown as it was normalized using experimental liquid permeability value. Details of permeability measurements are included in Appendix B. The experimental and numerical results shown in Fig. 7 indicate that the crushed Pyrophyllite sample should have an effective (or apparent) pore size equal to 20 nm. Fig. 8 shows the pore size distribution of the sample measured separately using high-pressure mercury porosimetry. Indeed, the sample has

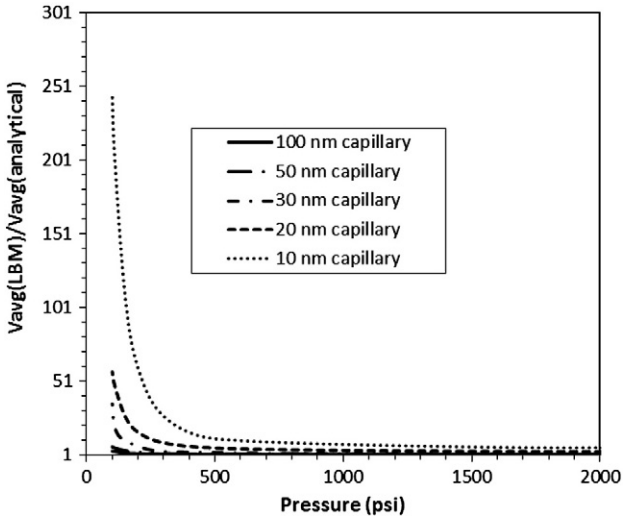

Fig. 4. Average gas flow velocity across nano-capillary for varying average pore pressure.

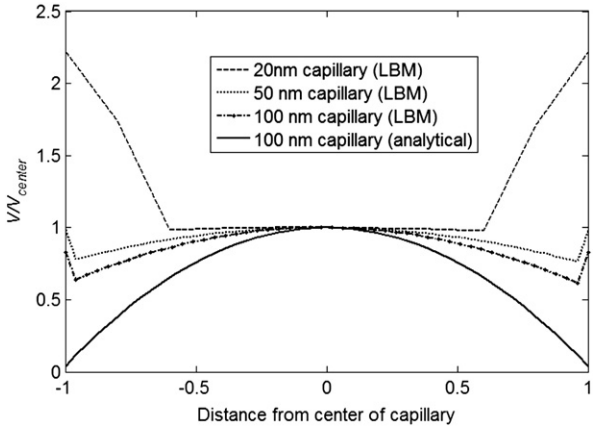

Fig. 5. Steady-state flow velocity profiles in capillaries with varying diameter at 100 psi average capillary pressure.

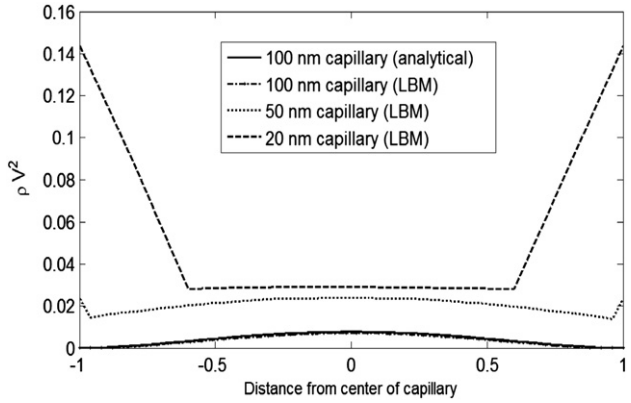

Fig. 6. Kinetic energy profiles of the steady-state flow in capillaries with varying diameter at 100 psi average pressure.

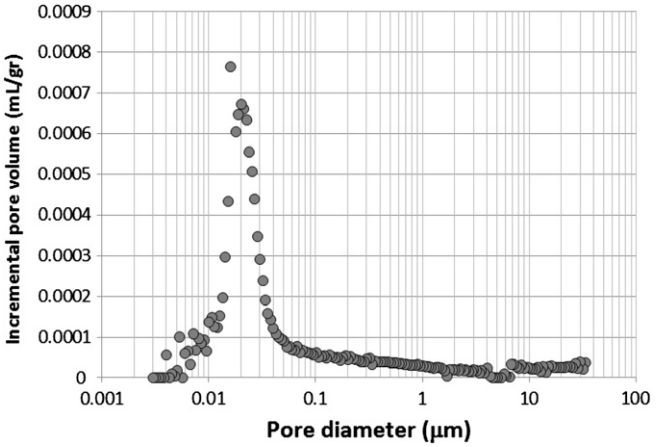

Fig. 8. Pore size distribution of the 5.68 mm Pyrophyllite sample using high-pressure mercury injection.

pores with sizes varying in a small range between 10 and 40 nm and dominated by 20 nm pores. Thus, the experimental and numerical data are consistent and their match is acceptable.

One could argue that the experimental data belongs to unsteady measurements and, hence, it should not be presented on the Klinkenberg chart. However, we show in Fig. 9 that, following the initial expansion of the introduced gas in the measurement cell, the recorded pressure decay across the cell is so small during the gas penetration into the fragments that the pressure value (inside the chamber, inside the particles, or at equilibrium) used in the Klinkenberg chart as the average pressure is nearly a constant.

In Fig. 10 we introduce a double-slip Klinkenberg chart that includes the permeability–pressure relationships for varying capillary sizes. Note that the apparent permeability of each capillary (K_a) is normalized with its corresponding absolute permeability (K), which is obtained using LBM simulation at 2500 psi (when no slippage could possibly occur), so that all the curves converge to unity at high pressures. It is clear that the kinetic effect of the gas molecules interacting with the capillary wall and the bulk is significant in capillaries with a diameter less than 50 nm. The effect is more pronounced when the capillary size is 20 nm or less.

3. Double-slip Klinkenberg equation for steady-state gas flow in nano-porous materials

The results of this study are applicable for many industrial and technological applications involving nano-porous materials. Measurement and prediction of the transport properties of low- and ultra-low permeability geological formations, such as in coalbed and organic-rich gas shale reservoirs are the main interest to the audience of this journal. Hence, we have followed a curve fitting approach in the previous section using the double-slip Klinkenberg chart (Fig. 10). Based on our numerical analysis, additionally we propose the following equation:

$$K_a = K\left[1 + \left(\frac{b}{p}\right)^2 \left(\frac{L_{Ke}}{\lambda}\right)\right] \tag{2}$$

Here, compared to the Klinkenberg's Eq. (1), the quadratic expression and the term inside the second parenthesis are new, capturing the kinetic effect of the gas molecules. λ is the mean free path of the gas molecules, which is influenced by the fluid type, pressure, and temperature, although it is not affected by the capillary size; b is a constant (as originally described by Klinkenberg); and b/p is equal to the ratio of the mean free path to the characteristic length of the capillaries: $4c\lambda/h$; finally, we introduce a new length scale (L_{Ke}) associated with the kinetic energy of the bouncing-back molecules. In large capillaries, the kinetic effect of the gas molecules is negligible, hence, (L_{Ke}/λ is in the same order as (p/b) so the Klinkenberg equation is valid, see Fig. 11; furthermore, at significantly high pressures, b/p in Eq. (2) goes to zero, such that $K_a \approx K$. The corresponding values for liquid permeability, Klinkenberg constant b, and (L_{Ke}/λ for different capillary sizes are provided in Table 1.

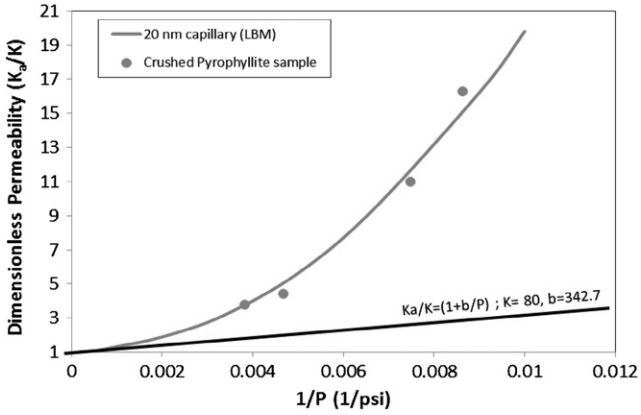

Fig. 7. Klinkenberg chart for steady-state gas dynamics in 20 nm capillary.

Fig. 12 (top) shows an example of history-matching of normalized permeability of Pyrophyllite sample 2 measured using gas uptake experiment. The measured normalized permeability values are following the straight line indicating that the Klinkenberg slip theory is valid for this sample and corresponding effective capillary size is larger than 100 nm. Fig. 12 (bottom) shows the pore size distribution of sample 2 using high-pressure mercury injection method. The mean pore size is more than 100 nm which is consistent with our observation using the double-slip chart. In Fig. 13 the application of the double-slip chart is shown for shale: sample #3. Normalized permeability measurements for this sample follow the trend for double-slip curve corresponding to 5 nm capillary, indicating the presence of double-slip effect on permeability measurements of shale sample #3. For this sample also high-pressure mercury injection confirms the effective pore size of less than 5 nm. We further validated the application of our double-slip chart using the permeability measurements of two more shale samples presented in Figs. 14 and 15. The normalized permeability values are following the double-slip curve corresponding

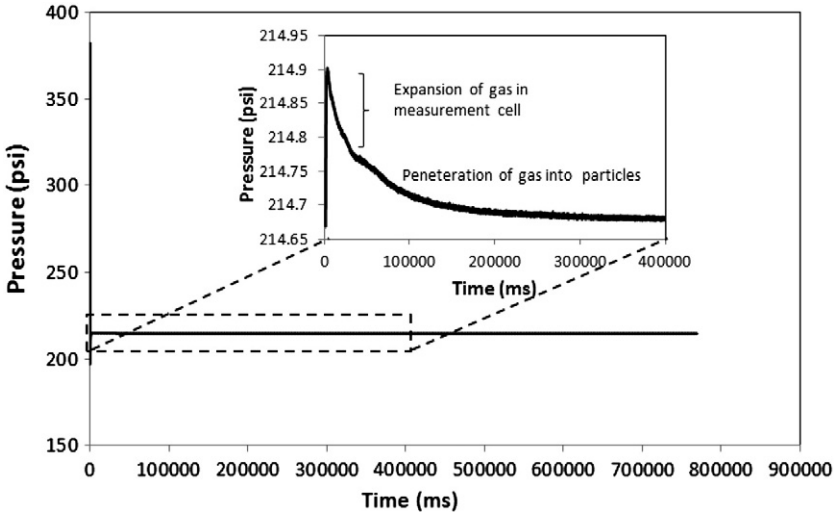

Fig. 9. Typical pressure decay during permeability measurement using crushed samples.

to an effective capillary size less than 5 nm which is again in good agreement with their effective pore size distributions obtained using high-pressure mercury injection.

4. Conclusions

A numerical investigation is presented showing that inelastic collisions of gas molecules with the nano-capillary walls create a high kinetic energy molecular streaming effect on the fluid flow. This leads to dramatic changes in the fluid flow velocity profile. As the consequence of these local dynamics, the apparent permeability of the nano-capillary is perceived as significantly higher than the absolute permeability. A double-slip Klinkenberg equation is proposed and a modified Klinkenberg chart is constructed to quantify the molecular streaming effect on the flow.

A practical significance of the presented theoretical work is on the measurement of crushed particle permeability using gas uptake or release experiments. The "crushed permeability" measurements for nano-porous coal and shale samples are routine for the unconventional natural gas industry. Unfortunately, although they are fast and low-pressure laboratory methods, there are widely-recognized uncertainties associated with these measurements mainly because the permeability varies significantly for the same sample when the results from different commercial laboratories are compared Passey et al. (2010). Often these differences in the reported values are attributed to the unknown laboratory conditions and measurement techniques, and size of the crushed sample fragments. In this work we showed that a dramatic variation in the apparent permeability is possible due to small changes in the measurement cell pressure due to kinetic effects of the gas molecules in nano-capillaries. We believe that the double-slip permeability concept and the modified Klinkenberg equation are likely to remove some of these uncertainties associated with the coal and shale permeability and lead to development of new measurement protocols for the industry.

The numerical and laboratory experiments presented in this article were designed such that adsorption of the fluid molecules on the capillary walls is negligible. The absence of this physical mechanism has led to a simplified and idealized environment where rigorous analysis on steady-state flow could be done. Considering more realistic problems in the presence of adsorption could lead to development of new phenomena, in particularly at high pressures. Consequently, one may need to consider the reduced capillary space available for flow and the adsorbed-phase transport (or surface transport) of the gas molecules during numerical and physical simulations. We left this investigation outside of the scope of this article due to space limitations. Further information on adsorption-dominated transport could be found in Fathi and Akkutlu (2011) and Akkutlu and Fathi (2011).

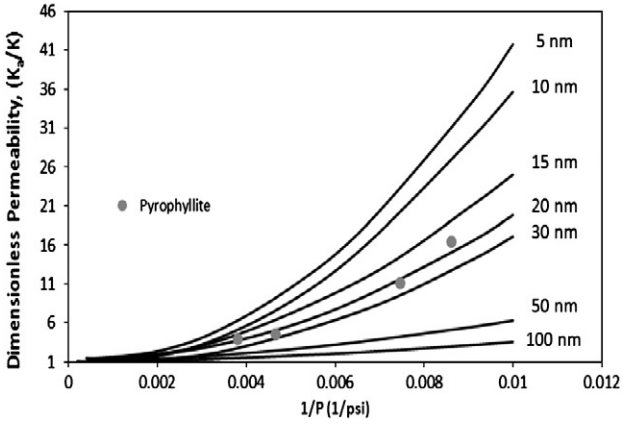

Fig. 10. Normalized double-slip Klinkenberg chart for steady-state gas flow in nano-capillaries and Pyrophyllite crushed permeability measurements.

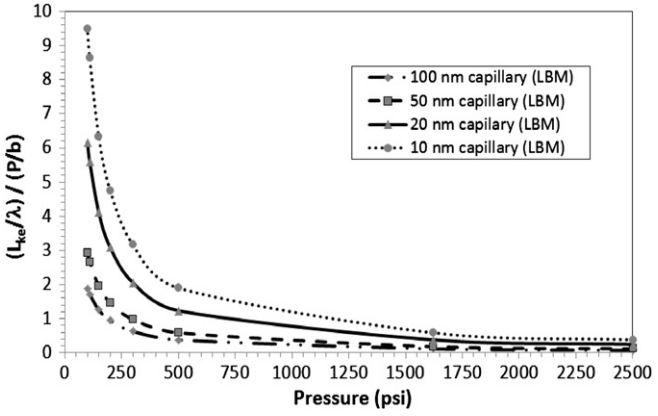

Fig. 11. $(L_{Ke}/\lambda)/(p/b)$ versus average pressure for varying capillary sizes.

Nomenclature

a	Lattice node
b	Slope of Klinkenberg straight line
c	Proportionality factor
e	Lattice velocity
f	Distribution function
f^{eq}	Equilibrium distribution function
G	Interaction strength
h	Diameter of capillary
K	Permeability
K_a	Apparent permeability
K_n	Knudsen number
L	Capillary length
L_{Ke}	Length scale of kinetic energy of bouncing-back molecules by the wall
N	Number of wall sites available for collision with the gas molecules
N_{Re}	Reynolds number
P	Pressure
R	Universal gas constant
T	Temperature
t	Time
V	Macroscopic velocity vector
V_{slip}	Slip velocity
V_{yi}	Velocity of gas molecule at site i in the (y-) direction of flow in the capillary
x	Lattice space

Greek symbols

λ	Gas molecules mean free path
μ	Gas dynamic viscosity
ρ	Gas density
τ	Relaxation time
τ^*	Effective relaxation time
υ	Gas kinematic viscosity
ω	Weighting factor
Ω	Collision operator
Ψ	Potential function
Π	relaxation time correction function

Appendix A. Lattice Boltzmann modeling of gas dynamics in straight capillary

LBM is a numerical method based on statistical physics, first developed for simulation of fluid dynamics and transport phenomena governed by the Navier–Stokes equations (Fathi and Akkutlu, 2011; Succi, 2001). Later LBM attracted great interest for the simulation of wide range of computational fluid dynamics problems (Nie, et al., 2002; Sukop and Thorne, 2006). LBM is described by the lattice Boltzmann equation, lattice pattern, and local equilibrium distribution function. The lattice Boltzmann equation is a combination of two processes: (i) streaming, in which each fluid particle moves in the direction of its velocity to the neighbor lattice node; and (ii) collision, where particles arriving at a node collide and change their velocity direction according to collision operator Ω. The lattice Boltzmann equation can be written as

$$f_a(x + e_a\Delta t, t + \Delta t) = f_a(x, t) + \Omega(f_a) \quad a = 0, 1, \ldots, N \tag{3}$$

Where f_a is the distribution function of particles, x and t are space and time dimensions, Δt is incremental time step, and e_a is the velocity vector of the particle at node a. The corresponding dimensions for location and time in LBM domain can be defined as lattice unit (lu) that is the fundamental measure of length in the LBM models and lattice time steps (ts) that is the time unit. The lattice Boltzmann equation (LBE) can be derived by discretization of Boltzmann equation in both time and space. In the lattice Boltzmann equation, the number of possible particle positions and their velocity directions is limited to the number of nodes in each lattice. The number of velocity magnitudes, which distinguishes different lattice patterns, is also limited. Further simplification of the general lattice equation has been made by assuming uniform particle mass (mu) equal to 1 that leads to equivalent microscopic velocities and momenta. Definition of the lattice pattern depends on the dimension of space we want to simulate; however, to recover the correct flow equations it is necessary to use specific lattice patterns that provide sufficient lattice symmetry, like

Table 1
Double-slip parameters for steady-state methane flow in nano-capillaries at 77 °F. The table is generated using LBM simulations.

Capillary Diameter h, nm	Liquid permeability, k, μd	b, psi	L_{KE}/λ
100	790	140	1.35
50	206	189	1.55
30	87	340	1.70
20	80	343	1.80
15	75	465	1.84
10	57	500	1.90
5	20	510	2.05

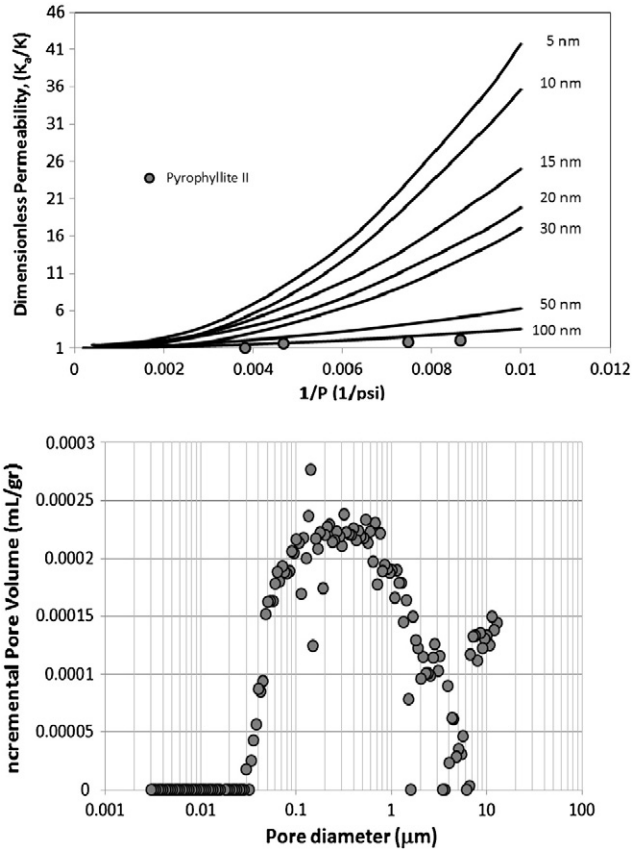

Fig. 12. Example history-matching of Pyrophyllite sample #2 using double-slip Klinkenberg chart and Procedure 2 at the top and pore size distribution of the sample obtained using high-pressure mercury injection at the bottom.

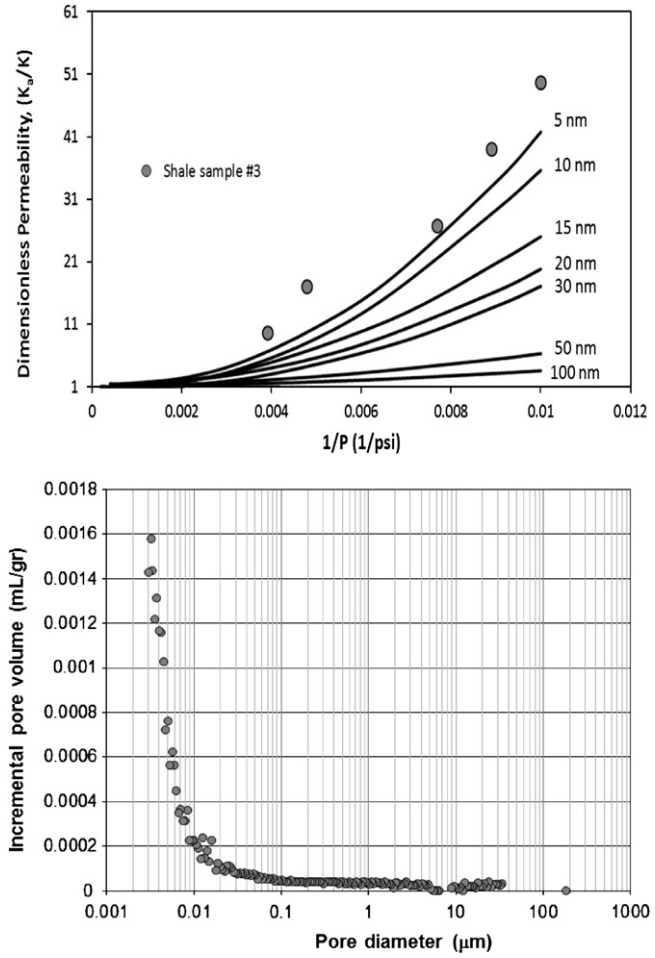

Fig. 13. Example history-matching of Shale sample #3 using double-slip Klinkenberg chart and Procedure 2 at the top and pore size distribution obtained using high-pressure mercury injection at the bottom.

square and hexagonal lattices (Sukop and Thorne, 2006). In two dimensional simulations, a 9 speed square lattice (Fig. 2; left) called D2Q9 has been used extensively, where each particle moves one lattice unit (lu) at its velocity defined by e_a (Eq. (4)) and in one of the eight directions indicated with 1–8 in Fig. 2 (left). Based on this nomenclature, the particle at position 0 is called the rest particle that has a zero velocity.

$$e_a = \begin{cases} (0,0) & a = 0 \\ \left[\cos\frac{(a-1)\pi}{4}, \sin\frac{(a-1)\pi}{4}\right] & a = 1,2,3,4 \\ \sqrt{2}\left[\cos\frac{(a-1)\pi}{4}, \sin\frac{(a-1)\pi}{4}\right] & a = 5,6,7,8 \end{cases} \quad (4)$$

The next step is to define a proper collision operator. The Bhatnagar–Gross–Krook (BGK) collision operator with a single relaxation time is often used for this purpose. The BGK collision operator is derived based on linearization of the collision operator around the equilibrium state, neglecting the higher-order terms, and assuming $\Omega_a(f_a^{eq})$ is equal to zero. Therefore, the BGK collision operator can be written as,

$$\Omega(f_a) = -\frac{f_a - f_a^{eq}}{\tau} \quad (5)$$

Here τ is the relaxation time which can be assumed constant in the case of nearly incompressible fluids. This assumption introduces the second order truncation error in the lattice Boltzmann equation. In isothermal LBM models this error is completely absorbed into the kinematic viscosity, υ, defined in (Sukop and Thorne, 2006) as:

$$\upsilon = (\tau - 0.5)RT \quad (6)$$

where R is the ideal gas constant and T is the temperature. In the D2Q9 model RT is taken to be equal to 1/3. Eq. (6) defines the relation between relaxation time and kinematic viscosity in continuum flow, suggesting flow is controlled by the Reynolds number, that is a non-dimensional number reflecting the balance between viscous and inertial forces and is inversely proportional to kinematic viscosity υ. However, in the case of transport in micro-channels with a large Knudsen number the flow is controlled by Knudsen number, which is defined as the ratio of the mean free path of molecules (λ) to the macroscopic length scale of the pores (h): $Kn = \lambda/h$. Therefore, the relaxation time needs to be corrected for the Knudsen number. Here we use the approach introduced in Suga, et al. (2010), where the effective relaxation time is a function of Knudsen number as follows:

$$\tau^* = \tau\Pi(Kn) \quad (7)$$

where the function $\Pi(Kn)$ is introduced as:

$$\Pi(Kn) = \frac{2}{\pi}\arctan\left(\sqrt{2}Kn^{-3/4}\right). \quad (8)$$

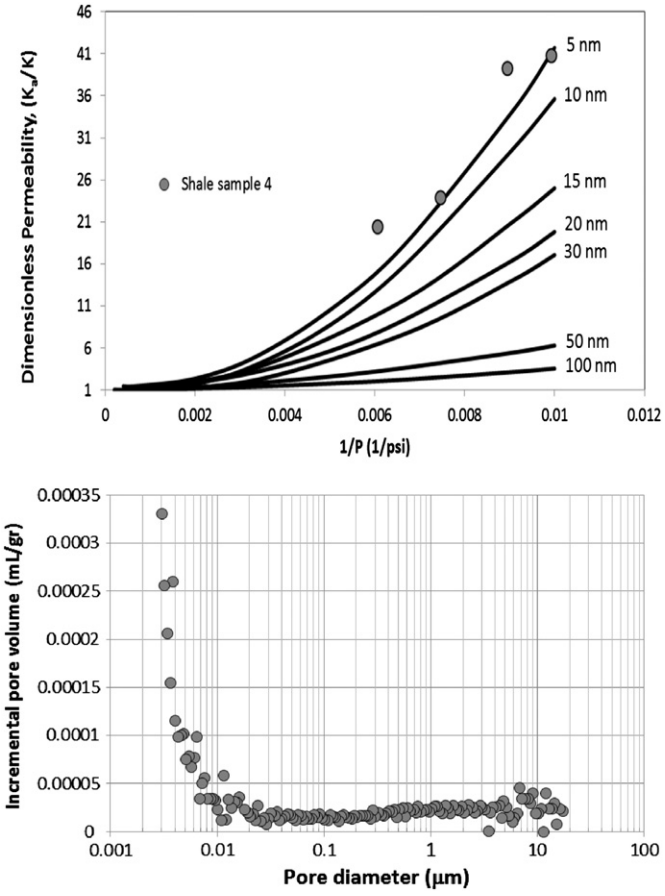

Fig. 14. Example history-matching of Shale sample #4 using double-slip Klinkenberg chart and Procedure 2at the top and pore size distribution obtained using high-pressure mercury injection at the bottom.

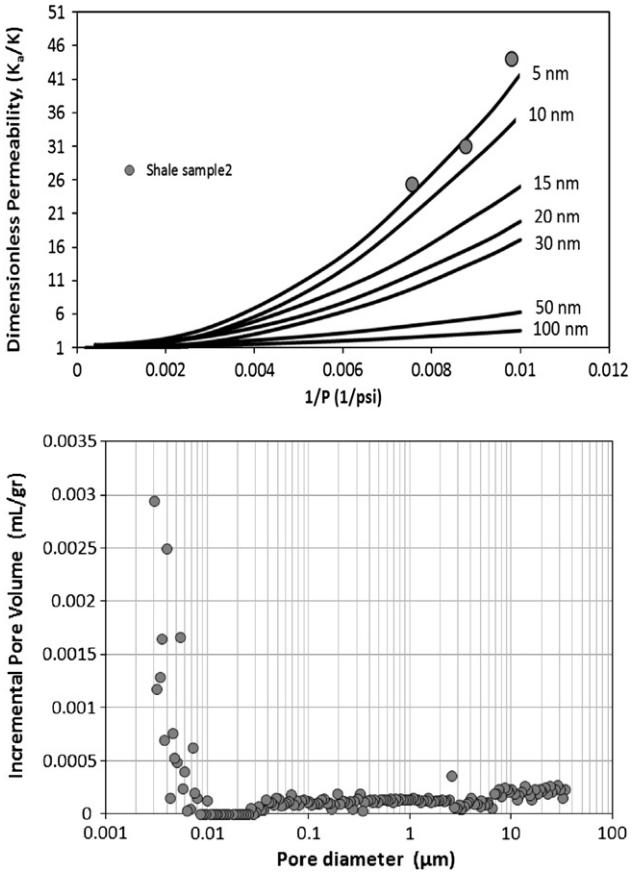

Fig. 15. Example history-matching of Shale sample #2 using double-slip Klinkenberg chart and Procedure 2 at the top and pore size distribution obtained using high-pressure mercury injection at the bottom.

The Knudsen number can be found using the following equation

$$Kn = \frac{\upsilon}{h}\sqrt{\frac{\pi}{2RT}}. \tag{9}$$

Application of Eq. (7) introduces the wall effect more clearly and implies that some of the particles hitting the wall have shorter effective relaxation time (τ^*) than the case where the wall effect was ignored (i.e. using τ instead), which appears as a mean slip velocity at the wall at the macroscopic level.

Having introduced the lattice Boltzmann equation and the lattice pattern, we are using equilibrium distribution function defined in Eq. (10) to solve Navier–Stokes problem.

$$f_a^{eq} = \omega_a \rho\left[1 + \frac{3(e_a \cdot V)}{e^2} + \frac{9(e_a \cdot V)^2}{2e^4} - \frac{3(V \cdot V)}{2e^2}\right]. \tag{10}$$

Here, the weights, ω_a, are equal to $\omega_0 = 4/9$, $\omega_1 = \omega_2 = \omega_3 = \omega_4 = 1/9$ and $\omega_5 = \omega_6 = \omega_7 = \omega_8 = 1/36$ and e is the lattice velocity defined as the lattice size (lu) over the lattice time step (ts). Gas density (ρ) and velocity (V) are macroscopic quantities that can be obtained as follows:

$$\rho = \sum_{a=0}^{8} f_a; \quad V = \frac{1}{\rho}\sum_{a=0}^{8} e_a f_a \tag{11}$$

A.1. Cohesive forces

To describe the interaction forces between the particles, we just consider the cohesive forces between neighbor particles and ignore the long range forces between them using the formulation introduced by Sukop and Thorne (2006):

$$F(x,t) = -G\Psi(x,t)\sum_{a=0}^{8}\omega_a \Psi(x + e_a \Delta t, t) e_a \tag{12}$$

Here, Ψ is the interaction potential function, G is the interaction strength that is negative for attractive forces, and ω_a is a weighting factor defined earlier in Eq. (10).

The interaction potential function can be defined as a monotonically increasing and bounded function. Here we use the simple form of the exponential function, where the interaction potential is a function of gas density and a constant ρ_0,

$$\Psi(\rho) = \rho_0\left[1 - \exp\left(\frac{-\rho(x,t)}{\rho_0}\right)\right] \tag{13}$$

Introduction of the interaction forces between the particles in the LBM formulation leads to non-ideal equation of state (Eq. (14))

$$P = \rho RT + \frac{GRT}{2}[\psi(\rho)]^2 \tag{14}$$

A.2. Boundary conditions

For the boundary conditions at the inlet and outlet we are using periodic boundary conditions where the capillary acts as a close system. In this case open ends are treated as if they are attached to opposite ends. Particles colliding with solid boundaries bounce off the boundary in such a way that their momentum in the direction of flow conserves and reverses perpendicular to the boundary (Poyurs, 2010). The body forces (cohesive forces) are added through the directionally-dependent force term in the equilibrium distribution that partially redistributes the particle motion at a node in the direction of the force term. These forces cause an extra momentum change to the particles in addition to the momentum exchange caused by collisions with other particles therefore the total momentum does not conserve locally; however, the momentum of the whole system can be shown to be conserved (Shan and Doolen, 1995).

Appendix B. Transient permeability measurement using crushed samples

The technique is commonly used to measure permeability of low-permeability crushed rock samples. Fig. 16 is a schematic of a

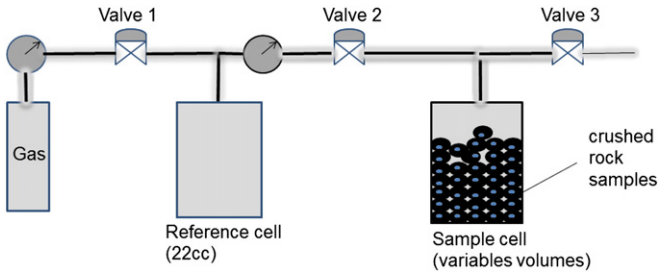

Fig. 16. Schematic of the apparatus used to implement the pressure decay measurement on crushed rock.

typical apparatus used for pressure decay measurement. The procedure is as follows. Initially valve 1 is closed when valves 2 and 3 are opened to the atmosphere. This is followed by the opening of valve 1 while valve 2 is closed and valve 3 remains open. Gas is allowed to flow and fill the reference cell at a predefined pressure. After the pressure in the reference cell has reached the thermal equilibrium, valves 1 and 3 are closed while valve 2 is opened. Gas is transported from the reference cell and expands into the sample cell and the sample particles. The pressure drop is continuously recorded with high precision digital pressure transducer during the gas expansion. The pressure transducer used allows sampling at high rates typically with a frequency of 4 ms.

In these experiments different gases such as helium, nitrogen or methane can be used to investigate the sieving effects. Because this experiment is usually performed under low pressures, gas adsorption is assumed negligible. Permeability is obtained by history-matching the transient pressure curve. This technique presents the advantage of being very fast compared to the other permeability measurement techniques, such as pressure pulse decay using core plugs, where the permeability dependency could also be investigated as a function of stress (Ousseini, 2012). Pulse decay measurements for core plugs under confining pressure can be used for that purpose. However it is very difficult to distinguish the velocity and permeability enhancement due to double-slip and stress effects using pulse decay experiment for core plugs under confining stress.

References

Akkutlu, I.Y., Fathi, E., 2011. Multi-scale gas transport in shales with local kerogen heterogeneities. SPE-146422-PP, paper presented during the SPE Annual Tech. Conf. Exhibition held in Denver, Colorado, October 30–November 2.

Fathi, E., Akkutlu, I.Y., 2011. Lattice-Boltzmann simulation of shale gas transport in kerogen. SPE-146821-PP, paper presented during the SPE Annual Tech. Conf. Exhibition held in Denver, Colorado, October 30–November 2.

King, M.R., 2007. Oscillatory gas flow in a circular nanotube. The Open Nanoscience Journal.

Klinkenberg, L.J., 1941. The permeability of porous media to liquid and gases. *Paper presented* at the API 11th mid-year meeting, Tulsa. API Drilling and Production Practices, New York, pp. 200–213.

Nie, X.B., Doolen, G.D., Chen, S.Y., 2002. Lattice-Boltzmann simulations of fluid flows in MEMS. Journal of Statistical Physics 107, 279–289.

Ousseini, T. Ali. 2012. Permeability measurements in nano-darcy rocks. Master's thesis submitted to Mewbourne School of Petroleum and Geological Engineering, University of Oklahoma.

Passey, Q.R., Bohacs, K.M., Esch, W.L., Klimentidis, R., Sinha, S., 2010. From oil-prone source rock to gas-producing shale reservoir — geologic and petrophysical characterization of unconventional shale gas reservoirs. SPE 131350 paper presented at the CPS-SPE International Oil and Gas Conference and Exhibition held in Beijing in China, June 8–10.

Poyurs, S.C. 2010. Application of the Lattice Boltzmann method to capillary seals and dynamic phase interface. Ph.D dissertation submitted to the Cornell University.

Shan, X., Doolen, G., 1995. Multi-component lattice Boltzmann model with inter particle interaction. arXiv:comp-gas/9503001v1.

Succi, S., 2001. The Lattice Boltzmann Equation for Fluid Dynamics and Beyond. Oxford University Press, Oxford.

Suga, K., Takenaka, S., Ito, T., Kaneda, M., Kinjo, T., Hyodo, S., 2010. Evaluation of a lattice Boltzmann method in a complex nanoflow. Physical Review E 82, 016701.

Sukop, M.C., Thorne Jr., D.T., 2006. Lattice Boltzmann Modeling: an Introduction for Geoscientists and Engineers. Springer, Heidelberg, Berlin, New York.